Maximum frontal speeds, alpha angles and deposit volumes of flowing snow avalanches

D.M. McClung, Department of Geography, University of British Columbia, Vancouver, British Columbia, V6T 1Z2, Canada

E-mail: mcclung@geog.ubc.ca

Tel: 604-822-3537

Peter Gauer, Norwegian Geotechnical Institute, Sognsveien 72, N-0855, Oslo, Norway

Abstract

Approximate maximum frontal speeds from 89 snow avalanches were analyzed to yield probabilistic estimates of maximum speed scaled with path length parameters. In addition to speeds, 88 companion values of runout for the events in terms of the alpha angle ($\tan\alpha = H_0/X_0$: total vertical drop / total horizontal reach) as a simple index of runout were analyzed and compared to the estimated frontal speeds. The results showed alpha angle decreases with maximum frontal speed but with wide scatter. Size estimates for 68 of the avalanches were obtained consisting of final deposit volumes. Correlation between speed and alpha angle measurements showed speed increases with size and alpha angle decreases with size. The probability estimates provided contribute to the definition of the design avalanche for a given avalanche path.

Keywords: snow avalanche, maximum speed, α angle, deposit volume

1. Introduction

A flowing avalanche is one which initiates as a slab and, if consisting of dry snow, will be enveloped in a low density turbulent snow dust cloud once the speed exceeds approximately 10 m/s. A flowing avalanche has a dense core of flowing material which dominates the dynamics by serving as the driving force for downslope motion. The core thickness is typically in the range of 1 -10 m which is on the order of about 1% of the length of the flowing mass. Due to the high flow densities in the core and high speeds, flowing avalanches can produce very high impact pressures. In applications, consultants require avalanche speeds to estimate impact pressures at locations along the incline or for design of defenses in the runout zone. For these applications, it is useful to have estimates of maximum frontal speed expected at some point on the path. Estimates of maximum speed can be used to characterize the design avalanche and for constraints on avalanche dynamics calculations and models. For example, if a dynamics model applied to the design avalanche yields a prediction of maximum speed much lower or higher than implied by speed data, questions should arise.

The conventional approach to avalanche dynamics consists of input of friction coefficients and parameters into a dynamics model to solve for speeds all along the path from start to runout position yielding a maximum estimate somewhere along the track. One purpose of our paper is to provide a risk-based probabilistic estimate of maximum frontal speed scaled with simple terrain scale variables to compare with maximum speed predictions.

In this paper, we present an extensive collection of estimated maximum frontal speeds of avalanches scaled with simple terrain length information with the aim of providing guidance for practitioners using avalanche dynamics models used to predict the maximum or design avalanche. Our method consists of fitting the ratios $u_m / \sqrt{S_0}$ and $u_m / \sqrt{H_0}$ (units: $m^{1/2}s^{-1}$) to probability density functions (pdf) where u_m is maximum downslope frontal speed (m/s), S_0 (m) is total path length traversed and H_0 (m) is total vertical drop for the events. Numbers $(u_m / \sqrt{gS_0}; u_m / \sqrt{gH_0})$ may be obtained by combining with g (magnitude of gravity acceleration). The analysis allows us to specify the ratios as a function of exceedance probability for applications.

In addition, we collected 88 values of runout in form of the α angle. Analysis showed increasing u_m implies farther runout or decreasing α. The Appendix contains a brief explanation of the α angle and its meaning as a simple index of runout as used in this paper. The variables: H_0, X_0, α are based on measurements for stop position of the individual avalanches not extreme values for the avalanche paths.

Size estimates of 68 of 89 avalanches were made from field reports of the final deposit volumes using the Europe Avalanche Warning Service scale (UNESCO, 1981). The results showed that u_m increases with *size* and α decreases with *size*. For the variables $(u_m, \alpha, size)$ comparisons reveal wide scatter in the results but with highly significant Spearman rank correlations with u_m.

2. Data description

We have collected estimates of maximum frontal speed u_m from 89 avalanche events. The analysis is given here to provide practitioners with estimates the maximum speed scaled with some measure of the terrain scale over which the avalanches ran. We have chosen two measures ($\sqrt{H_0};\sqrt{S_0}$) for scaling, from McClung (1990), McClung and Schaerer (2006) and Gauer (2013; 2014). Our data consist of 89 avalanches with H_0 and S_0 estimated. Of these, we have 30 values from Europe and Japan with H_0,S_0 and u_m estimated accurately since the avalanche speeds were determined at all or nearly points along the paths all along the path. The remaining (59) are from Canada with approximate estimates of u_m from timing the avalanche motion over a known section of the path where approximate maximum speed is expected. The data (Table 1) are from Canada, Norway, Switzerland, Russia, Italy, Austria and Japan and are described by: Schaerer (1975), McClung and Schaerer (1983), McClung (1990) and Gauer (2013, 2014). Field observations showed that 79 % of avalanches with debris water content recorded had dry debris. Water content of the debris is analyzed below in a separate section. Separate descriptions of the Europe-Japan (30 events) and Canadian (59 events) data sets are given below.

2.1 Description of Canadian data

The Canadian data set was derived from field measurements from 59 avalanches on 26 avalanche paths collected in the area of Rogers Pass, Selkirk Mountains, British Columbia. The Canadian data were partly described by Schaerer (1975) and McClung and Schaerer (1983). The data were taken by timing over steep sections of the paths well away from the starting zone areas where most acceleration takes place and well away from the runout zones where most deceleration take place. The speeds were determined by timing with a stopwatch over sections of the path which were straight and between prominent recognizable terrain features. The data consist of single speed estimates instead of full profiles. Thus, the data accuracy is not nearly as good as data determined by precision methods such as radar by Gubler et al. (1986), photogrammetry (Kotlyakov et al., 1977) or films (Bakkehøi et al, 1983). For the Canadian data, the speed estimates were determined by visual observations so use of the data contains the approximation that the frontal speed is the same as the dense core of the avalanche for the dry and moist avalanches. For avalanches with wet debris, the core was visible with the avalanches having no (wet) snow dust cloud. All Canadian events were triggered by gun fire (recoilless rifle and howitzer) from the valley bottom.

The mean and median slope angles over which the Canadian measurements were taken was 33^o with a range : $20^o - 50^o$ (59 values). The terrain at Rogers Pass is such that for some avalanche paths a region exists below the starting area which is steeper than the starting area itself (Schleiss, 1989). Of the 26 avalanche paths, 14 had gully features and 12 had open slopes in the track (Schleiss, 1989) where the measurements were taken. All 26 paths had wide open slopes in the runout zone. McClung and Schaerer (2006) have given descriptions of the avalanche track and runout zones of avalanche paths. Accounting for three dimensional terrain features is beyond the scope of this paper.

All cases included notes on the mass and volume of the avalanche deposits whether small, medium, large or major. In addition, field estimates of the length, width and depth of the deposits were made for a majority of the avalanches. The latter gave volume estimates for 42 avalanches (31 dry, 5 moist, 6 wet) ranging from 160 – 61,000 m^3 with a median: 2100 m^3. Only avalanches with deposit dimensions could be used in size estimates below.

In addition to approximate avalanche speeds, α angles were recorded for all 59 avalanches based on the tip of the debris and the starting position (see the Appendix). For the α angle analysis and the speed estimates, maps of scale 1: 5000 with 5 m contours were used. The path scales (H_0, S_0) were determined from the distal end of the avalanche debris combined with maps of scale 1:5000.

2.2 Description of Europe – Japan data

The 30 events from 10 different avalanche paths from Europe and Japan all had profiles of the speed distribution along the track (or central portions) of the paths. Brief descriptions of events are found in Gauer (2013; 2014) and references therein. The European data were from Italy (1 event), Switzerland (13 events), Japan (1 event), Russia (1 event), Norway (12 events), Austria (2 events). Twelve of the events were recorded at the Ryggfonn path, Norway (Gauer, 2013, 2014) and 5 events were from Vallée de la Sionne, Switzerland (Gauer, 2013, 2014). The test sites at Ryggfonn and Vallée de la Sionne are described by Barbolini and Issler (2006). Data were collected by photogrammetry, films and radar. For the photogrammetry and films, the approximation was made that frontal speed was the same as the dense core. The measurements were made between: 1975 – 2010. One avalanche had wet debris, 28 were classed as dry with one event from the Khibins, Russia (Kotlyakov et al, 1977) having unknown water content of debris.

3. Probability analysis results

The descriptive statistics for u_m, α and scaled ratios are given in Table 1.

Table 1: Descriptive statistics of the continuous variables for all events (89).

Variable	u_m(m/s)	$u_m / \sqrt{S_0}$ ($\mathrm{m}^{1/2} s^{-1}$)	$u_m / \sqrt{H_0}$ ($\mathrm{m}^{1/2} s^{-1}$)	S_0 (m)	H_0 (m)	$\alpha(^o)$
N	89	89	89	89	89	88
Max	70	1.5	2.2	3600	1940	45
Min	8	0.2	0.2	170	100	20
Median	30	0.9	1.1	1680	900	32
Mean	32	0.8	1.1	1640	890	32
Std. Dev.	15	0.3	0.5	670	340	5

Table 1 shows that the speed variables all vary by about a factor of 10. Similarly, the scale variables $(S_0; H_0)$ and $\alpha(^o)$ encompass wide ranges.

The first part of our analysis consists of fitting the values of $u_m / \sqrt{H_0}; u_m / \sqrt{S_0}$ to probability density functions (pdf) to estimate the exceedance probability for the scaled ratios. In general, we found the best fits for the larger data sets to fit a beta pdf and for the subset of 30 scaled with $\sqrt{H_0}$, we found a Log Pearson 3 (LP 3) pdf was best. The LP 3 pdf is given by (Vogel and McMartin, 1991):

$f(x) = \frac{1}{x|\beta_0|\Gamma(a)}\left(\frac{\ln(x)-\gamma}{\beta_0}\right)^{a-1} \exp\left(-\frac{\ln(x)-\gamma}{\beta_0}\right)$ where (a, β_0, γ) are non-integer constants and $\Gamma(a)$ is the gamma function.

All pdfs in this paper were derived from fitting the values to 60 different pdfs considering five goodness-of-fit criteria: three goodness-of-fit statistics: K-S (Kolmogorov-Smirnov); A-D (Anderson-Darling) and C-S (Chi-squared) plus probability plots (P-P) and quantile plots (Q-Q).

All (P-P) and (Q-Q) plots had adjusted coefficient of determination $R^2 \geq 0.98$ for the linear fit through the data points by inspection (Figure 1).

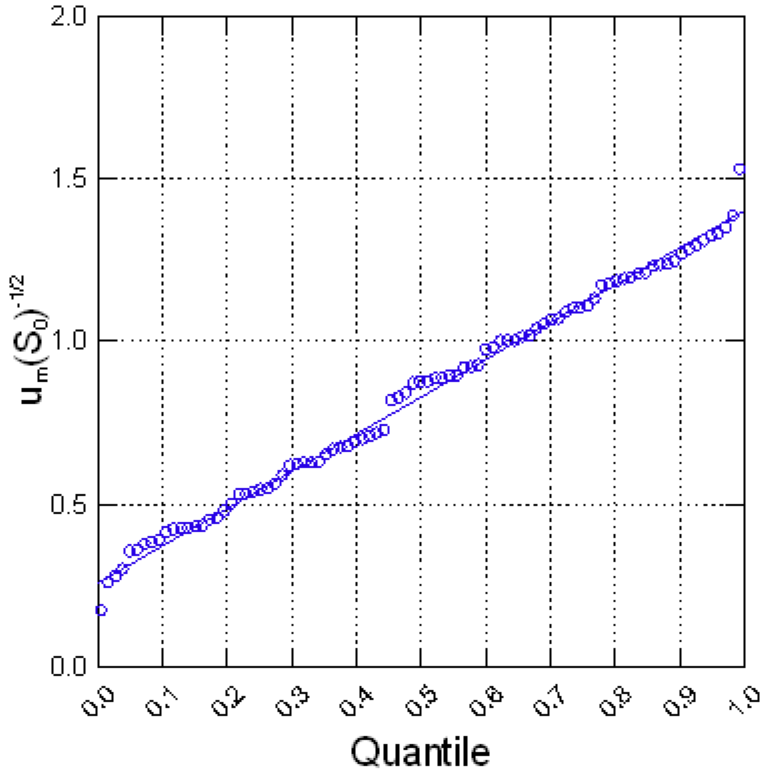

Figure 1 : $u_m / \sqrt{S_0}$ $(m)^{1/2} s^{-1}$ versus Quantiles for the beta distribution (N = 89). The calculated distribution parameters are: min: 0.14, max: 1.56, shape factors: 1.80, 1.93.

Table 2 contains a summary of the results including the values of the scaled ratios for 1%, 5% and 10% probability of exceedance and comparison of the three statistics with critical significance values.

Table 2: Scaled ratios versus (%) exceedance probabilities, best fitting pdfs, and values of the K-S, A-D and C-S statistics compared with their critical values for level of significance $\alpha_s = 0.2$ in parentheses. Calculations are given for all avalanches (N = 89) and Europe – Japan (N = 30).

N	Ratio	pdf	1%	5%	10%	K-S	A-D	C-S

30	$u_m/\sqrt{S_0}$	beta	1.5	1.4	1.3	0.09(0.19)	0.19(1.37)	0.32(4.64)
89	$u_m/\sqrt{S_0}$	beta	1.5	1.4	1.3	0.06(0.11)	0.44(1.37)	1.93(8.56)
30	$u_m/\sqrt{H_0}$	LP 3	2.3	2.1	2.0	0.06(0.19)	0.11(1.37)	0.04(5.99)
89	$u_m/\sqrt{H_0}$	beta	2.2	2.0	1.9	0.05(0.11)	0.31(1.37)	6.66(8.56)

The results (Table 2) suggest that the ratio $u_m/\sqrt{S_0}$ has more consistent values for the two data sets. The ratio $u_m/\sqrt{S_0}$ (Fig. 1) might be preferred over $u_m/\sqrt{H_0}$ for illustrating applications since path length enters directly into avalanche dynamics (Newton's 2nd Law) when entrainment and non-conservative forces such as rapid, dynamic, Coulomb friction are applied to model flowing avalanches. However, some may prefer to use $u_m/\sqrt{H_0}$ since H_0 may be easier to determine. Spearman rank correlation of u_m vs $\sqrt{S_0}$ gave 0.49 (p < 0.0005) and for u_m vs $\sqrt{H_0}$ it was 0.26 (p = 0.005). All significance values (p) for Spearman's rank correlation coefficient (r_s) in this paper were determined by calculation of the t-statistic (Harnett, 1975) as:

$t = r_s\sqrt{(N-2)/(1-r_s^2)}$ using tables of the t statistic and $p < 0.05$ to achieve significance.

The Canadian data (59) analyzed with 60 distributions for $u_m/\sqrt{S_0}$ gave: 1.6 (1%); 1.3 (5%) and 1.1 (10%) with K-S : 0.07(0.14); A-D: 0.29 (1.37) ; C-S: 0.64 (7.29) with $\alpha_s = 0.2$ for the best fitting LP 3 pdf.

Figure 2 shows the 1 % exceedance line $(u_m = 1.5\sqrt{S_0})$ comparison with the data. The values which come closest to the line are from Norway (41 m/s: dry debris but stopped in the track) and

Canada (17, 18 m/s: both wet debris). Figure 2 suggests that some of the Canadian data contribute to the 1% exceedance probability line but many are below the line. The decline of the slope of the asymptote line with increasing exceedance probability (5%, 10%) analyzed above is due to the larger number of avalanches with lower ratios of $u_m / \sqrt{S_0}$ than for the Europe – Japan data. It is shown below that the Canadian avalanches were, on average, of smaller size and more contained moist and wet debris.

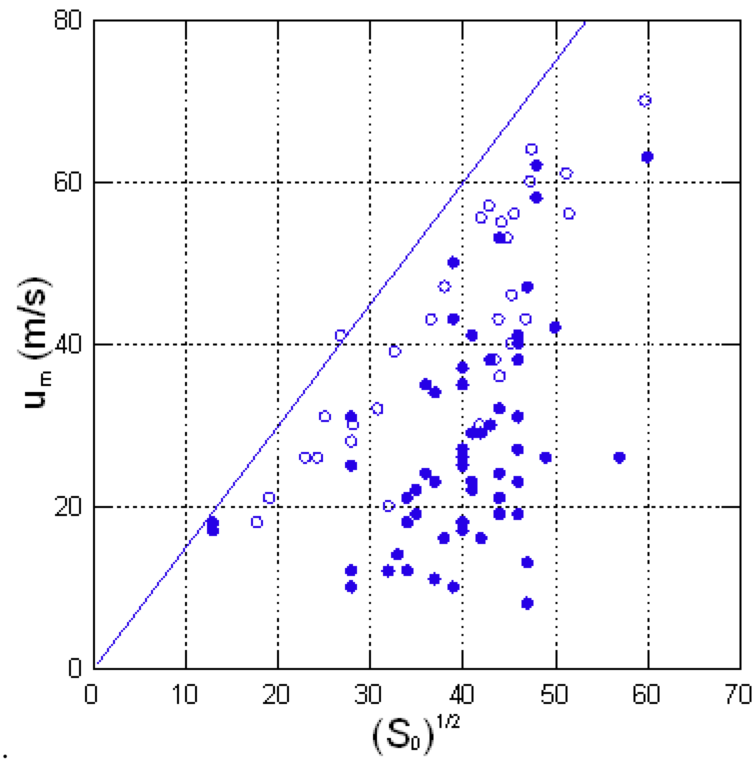

Figure 2: A plot of u_m (m/s) versus $\sqrt{S_0}$ $(m^{1/2})$ with a line drawn representing $u_m = 1.5\sqrt{S_0}$ (1% exceedance) for N = 89. The symbols ●,○ represent Canadian and Europe – Japan data respectively.

Figure 2 suggests there are limitations with respect to practical use of the single variable asymptote ($u_m = 1.5\sqrt{S_0}$). We suggest that the approximate limits on usage are:

$10\ m^{1/2} < \sqrt{S_0} < 50\ m^{1/2}$ due to a scarcity of data beyond these limits. The two events with $\sqrt{S_0} = 60\ m^{1/2}$ are the largest and fastest in the data base from Switzerland (Vallée de la Sionne), (70 m/s) and Canada (Ross Peak) (63 m/s) and the 1% asymptotic line is well above the speeds for these events. The *size* of the avalanches is presented in Section 5.

4. Relation of u_m and α angles

In addition, to: $u_m / \sqrt{H_0}$; $u_m / \sqrt{S_0}$, we also provide values of the α angle (Table 1) for runout positions calculated from start position to stop position of the tip of the avalanches. The α angle is a very simple measure of runout introduced by Heim (1932) and used by Scheidegger (1973) for rock avalanches. The Appendix contains a description of the α as a simple index of runout.

Figures 3 - 5 contain information about the measured α angles.

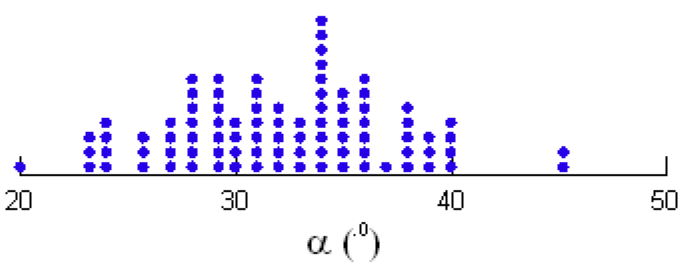

Figure 3: Dot histogram of 88 measured α angles.

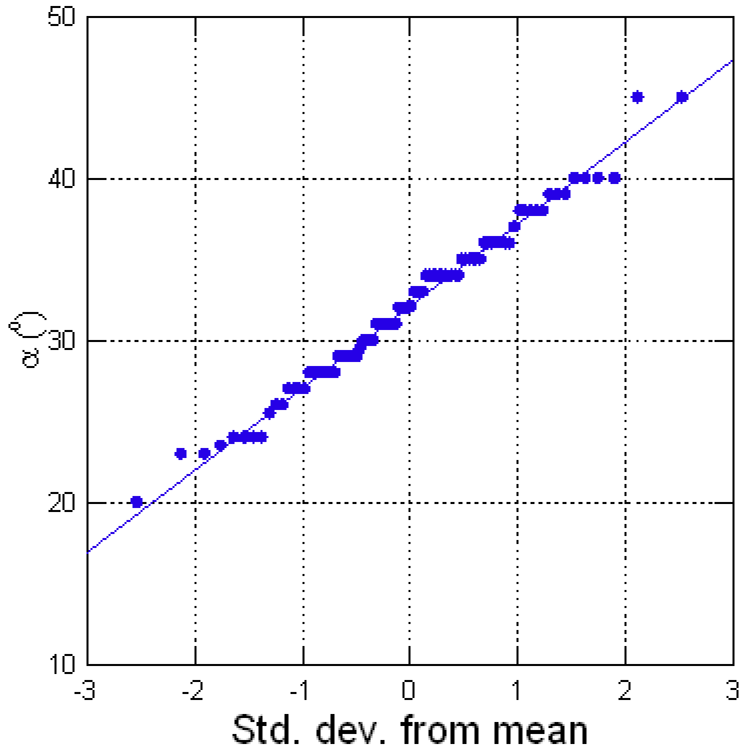

Figure 4: Normal plot of $\alpha(^o)$ vs. quantiles in standard deviations from the mean for 88 events.

Figure 4 shows that α follows a normal distribution ($R^2 = 0.99$). Goodness of fit statistics and critical values for $\alpha_s = 0.2$ are: K-S: 0.09 (0.11), A-D: 0.34 (1.37), C-S: 3.44 (8.56). The range of α (Fig. 3) suggests our data set reflects a wide range of typical avalanche situations.

McClung and Mears (1991) collected α angles from more than 500 paths with maximum runout estimated for return periods on the order of 100 years and the range of values was: $14^o - 42^o$ which is different than that in Table 1: $(20^o - 45^o)$. The mean values for different mountain ranges from McClung and Mears (1991) ranged from $20^o - 28^o$ compared to 32^o in Table 1. The differences are due to the selection of extreme runout positions estimated to be of the order of 100 year return period (varying between about 50 and 300 years) by McClung and Mears (1991) compared to the population of avalanches with speed data measured in the present study which do not all represent extreme events for runout.

Figure 5 shows u_m versus α for 88 avalanches. The rank correlation is -0.54 ($p < 0.0005$). It shows general decrease in α with increasing speed. Very wide scatter is shown. Figure 5 is a depiction of the correlation result and it is not a model. It is shown below (Section 5) that α is a weak predictor of u_m in combination with $size$.

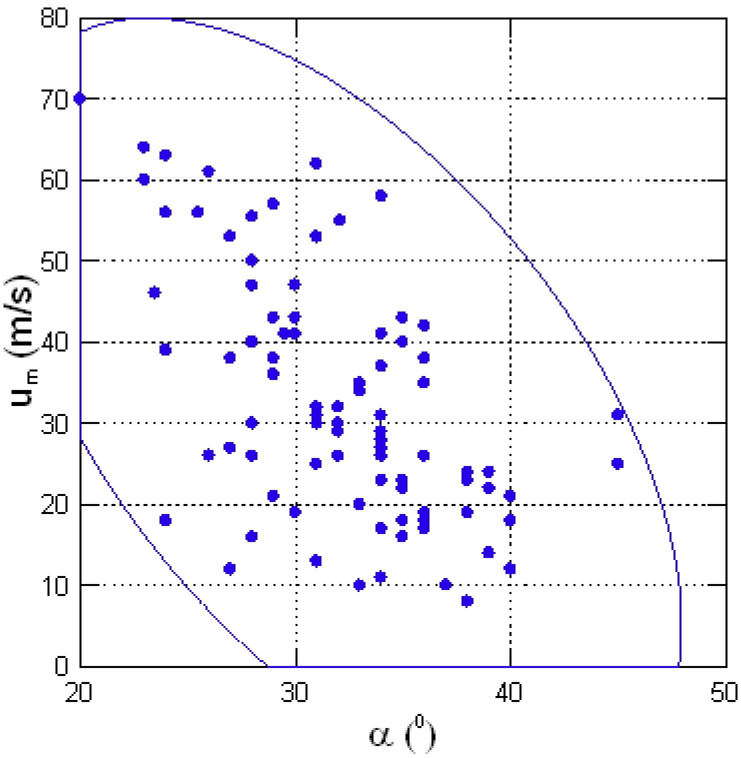

Figure 5: Measured values of u_m vs. α. A 99% confidence ellipse is shown.

We also fit u_m to 60 distributions (89 values) and we found a three LP 3 pdf gave the best fit. Goodness of fit statistics and critical values for $\alpha_s = 0.2$ are: K-S: 0.05 (0.11), A-D: 0.31 (1.37), C-S: 2.03 (8.56). The distribution u_m had statistically significant positive skewness with the ratio of skewness to standard error of skewness equal to 2.2. The pdf results for $u_m;\alpha$ suggest that these two variables are non-linearly related for our data set since they follow different pdfs.

Rank correlations of α vs. $u_m/\sqrt{S_0};u_m/\sqrt{H_0}$ are - 0.46; - 0.58 (both with p < 0.0005). Rank correlation of $(\alpha,\sqrt{S_0});(\alpha,\sqrt{H_0})$ gave: -0.35, p <0.0005; -0.06, p >0.10 respectively. The results showed that α has highly significant negative correlation with $\sqrt{S_0}$ but insignificant correlation with $\sqrt{H_0}$.

The quotient variable $(u_m/\sqrt{H_0})$ has nearly the same correlation (-0.58) with α as $u_m/\sqrt{S_0}$ (-0.54; Figure 5). Since α has insignificant correlation with $\sqrt{H_0}$, the quotient $u_m/\sqrt{H_0}$ gives almost the same correlation result as Figure 5 and is similar to dividing u_m by a constant. This result implies the quotient variable ($u_m/\sqrt{H_0}$) does not yield any more information than u_m for correlation with α. For both variables in Figure 5, the correlation with $\sqrt{S_0}$ is higher than with $\sqrt{H_0}$.

5. Deposit volume estimates compared with u_m and α angles

As an index of avalanche size, we used the volume scale from the European Avalanche Warning Service (EAWS) (UNESCO, 1981). We placed the volume (V) of the deposit (m^3) into 5 size classes defined by: $size = \log_{10}(V) - 1$ by orders of magnitude for $size$ 1-4 where e.g. $size\ 1 = 100\ m^3$, $size$ 4=100,000 m^3 and $size$ 5 >10^5 m^3. The 42 of 59 Canadian avalanches with size data were transformed by the formula and placed in the categorical size bins. The bin estimates were placed by rounding up or down to the nearest size class. For example, size 2.4 was classed as size 2 and size 2.6 was classed as size 3. For the 26 avalanches from Europe and Japan with sizes recorded, the same procedure was followed. However, for some cases, an order of magnitude volume was given with the field report instead of deposit dimensions so that estimate was used for bin placement. It is important that the size estimates are the final volume of the deposit. Sovilla et al. (2006) showed that entrainment during descent can increase the initial volume by up to a factor of 10. Figure 6 shows a dot histogram for the 68 values. Counts for individual size classes (1-5) were: (1,23,16,2,0) for the Canadian data and (2,3,12,7,2) for the European- Japan data.

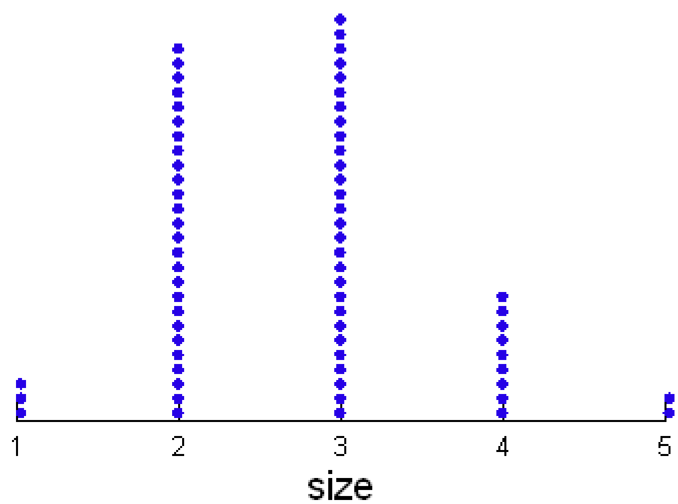

Figure 6: Dot histogram for 68 avalanches with EAWS size estimates.

Figure 7 shows a plot of maximum speed versus the categorical size for 68 avalanches. The rank correlation was 0.69 ($p < 0.0005$). It implies speed correlates positively with size, with upper values of speed increasing with each size class. It also shows wide variations of speed within size 2 and size 3 where most of the data lie. Linear regression gave:

$$u_m = 12.2(size) + 10.2(\mathrm{N}_{P_E}) \qquad (1)$$

with $R^2 = 0.54$ and N_{P_E} as the number of standard deviations from the mean for a given % exceedance probability for a normal distribution. The standard error is 10.1 m/s, and $N_{P_E} = 2.32\ (1\%);\ 1.65\ (5\%);\ 1.28\ (10\%)$ to yield upper limit estimation in a probabilistic sense for a given size. A probability plot of the residuals showed they had a good fit to a normal distribution to enable the approximate probability estimates. Regression with a constant showed the constant was not significant statistically. The expression relating $u_m, size$ is a standard confidence limit equation with best accuracy for data rich size classes (2,3) but not for the data sparse sizes (1,5). The low value of R^2 implies the confidence equation is of limited value.

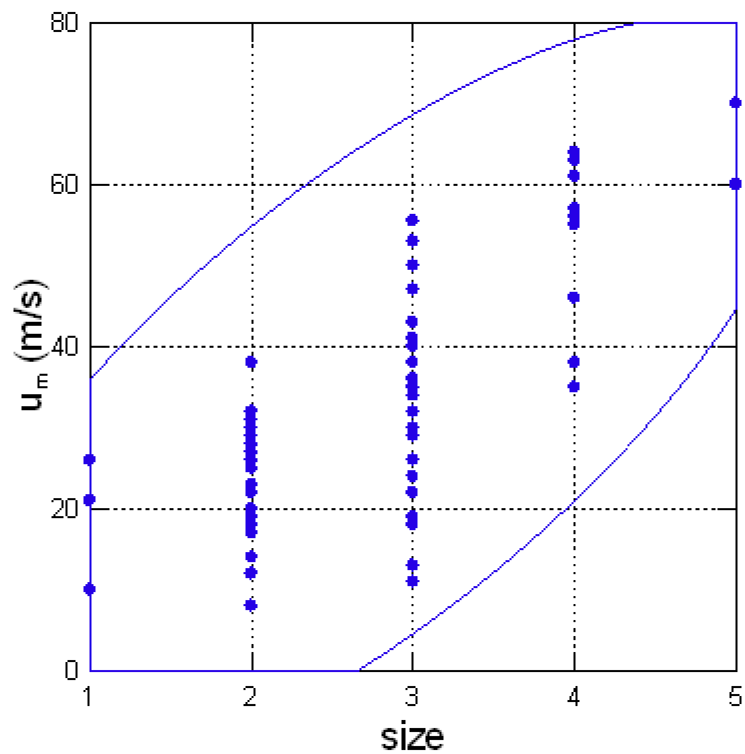

Figure 7: Plot of u_m versus $size$ for 68 avalanches with a 99% confidence ellipse.

Multiple regression confidence equations were determined, as above, for u_m with respect to the two runout variables $(\sqrt{S_0}, \alpha)$. These gave:

$$u_m = -10.4 + 0.33\sqrt{S_0} + 11.2(size) + 9.9\,\mathrm{N}_{P_E} \quad (\mathrm{R}^2 = 0.57) \qquad (2)$$

and

$$u_m = 38 - 0.97\alpha + 9.6(size) + 9.4N_{P_E} \quad (R^2 = 0.61) \qquad (3)$$

For both (2) and (3), $size$ is the stronger of the predictor variables. For (2), the t-statistics are: 7.1 $(size)$ and 2.4 $(\sqrt{S_0})$ and for (3), they are: 5.9 $(size)$ and -3.6 (α).

For $size$ 4 and 5 with $\sqrt{S_0} = 60\ m^{1/2}$ (Fig. 2) and 1% exceedance, the calculations (2) give: 78 m/s ($size$ 4) and 89 m/s ($size$ 5) compared with measured values 63 m/s (Ross Peak, Canada) and 70 m/s (Vallée de la Sionne, Switzerland) for $size$ 4 and 5 respectively. The calculated values are comparable to the 99% (1% exceedance) confidence ellipse in Figure 7 based only on u_m. Use of the confidence equation (1) with $u_m, size$ gave 72 m/s ($size$ 4) and 85 m/s ($size$ 5). Given the uncertainties, we suggest the multiple regression equations are of limited value since the differences in estimates are small compared with equation (1) and the expected uncertainties.

Figure 8 shows a plot of α angles versus categorical $size$ for 68 avalanches. It shows a general increase in α angle with decreasing size. The rank correlation is -0.54 ($p < 0.0005$). Again, sizes 2 and 3 show wide variations of α angle. Except for size 1, the plot indicates maximum α angle within a size class increasing with decreasing size. Linear regression of α versus $size$ gave a low coefficient of determination: $R^2 = 0.31$. Linear regression of α versus u_m gave: $R^2 = 0.32$ for 88 avalanches. Multiple regression of α versus u_m and $size$ showed that the $size$ was not statistically significant (p = 0.18) in combination with u_m $(R^2 = 0.41)$. Mixing the categorical $size$ variable with random variables (α, u_m) affects the regression and correlation results (Figures 7 and 8).

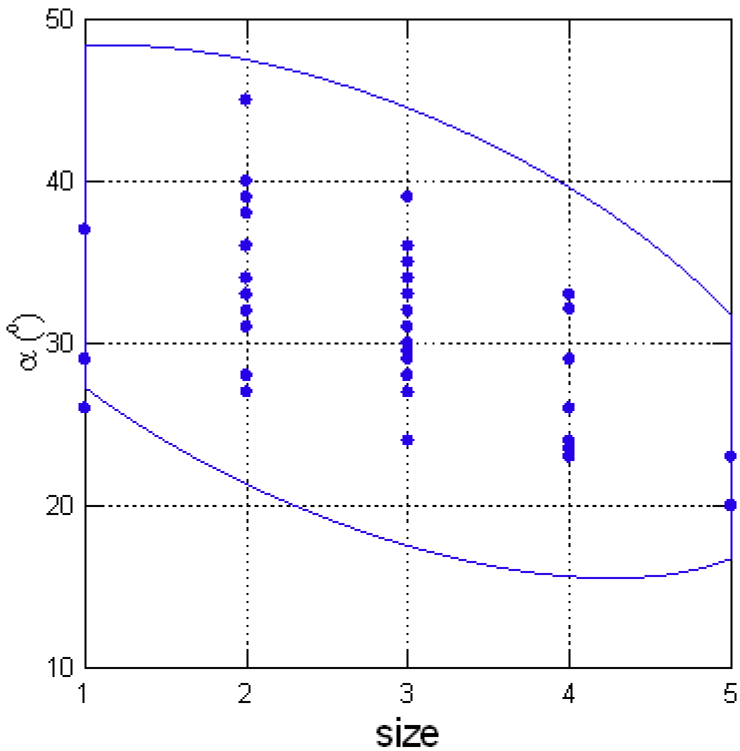

Figure 8: Plot of α angles versus size for 68 avalanches with a 99% confidence ellipse.

Figures 7 and 8 are graphical illustrations of the rank correlations given. They do not constitute models. However, they suggest that larger avalanches in general attain higher speeds (Fig. 7) and larger avalanches tend to imply smaller α angles (Fig. 8).

6. Water content of debris

For 86 of the 89 avalanches, descriptions were made in relation to the water content (dry, moist, wet) observed for the flowing mass and inspection of the avalanche deposits. Our data included 79% (68 events) classed as dry, 13 % (11 events) as wet and 8% (7 events) as moist or mixed. The median and range of speed values were: 31 m/s (8 – 70 m/s) (dry), 17 m/s (10 – 42 m/s) (wet) and 24 m/s (12 – 53 m/s) (moist). For the Canadian data, 42 were classed as dry, 10 wet and 7 moist. Since the numbers of avalanches with wet or moist debris are small compared to those dry, analysis of the separate classes was felt to have limited use. A t-test for the means of u_m for dry and wet avalanches gave t = 3.20 with 19 degrees of freedom ($p < 0.005$) which implies a significant difference between the means: 34 m/s (68 dry events) and 20 m/s (11 wet events). However, for different deposit volumes, the analysis is not meaningful since the differences are affected by the *size*. For the 56 dry events with *size* estimated, the median size was 3 (mean 2.8) whereas for the 7 wet events with *size* the median was 2 (mean 2.4). A t-test for the moist and wet avalanches gave no significant differences between the means of u_m. Grouping moist and wet avalanches together gave a significant difference ($p = 0.007$) between the means of u_m: 34 m/s (68 dry events; median *size* 3) versus 24 m/s (18 moist and wet events; median *size* 2) with a t-statistic 2.9 ($p = 0.007$). Again, the *size* differences between the groups prevent a meaningful comparison. Most important may be the highest speeds estimated for wet (42 m/s) [no size recorded] and moist (53 m/s) [size 3] events.

Probability analysis of the 68 dry events with $u_m / \sqrt{S_0}$ for 60 distributions gave a best fit with an error distribution using the 5 goodness of fit tests as above. The pdf of the error distribution is given by: $f(x) = c_1 \sigma^{-1} \exp(-|c_0 z|^k)$ with $z = (x - \mu)/\sigma$ with k, σ, μ as shape, scale and location parameters. The constants are: $c_0 = \left(\Gamma(3/k)/\Gamma(1/k)\right)^{1/2}$ and $c_1 = kc_0/2\Gamma(1/k)$. Fit statistics for $\alpha_s = 0.2$ with critical values in parentheses gave: K-S : 0.07(0.13), A-D: 0.24(1.37),C-S: 0.75 (8.56). The values of $u_m/\sqrt{S_0}$ with % exceedance probability were: 1.5 (1%), 1.4 (5%) and 1.3 (10%) which are the same as for the analysis for all events (Table 2). A very good fit was also obtained for a beta pdf.

7. Comparison of the Canadian and European - Japan data sets

All 59 of the Canadian speed data were collected in the same way by timing over steep terrain over recognizable sections of the path in the same mountain range. The 30 avalanches from Europe and Japan with more complete speed profiles were collected in Italy, Norway, Switzerland, Austria and Russia using radar, films and photogrammetry. Taken as two separate data bases, the Canadian and European-Japan data are compared here. The basic variables include: α angles, u_m and *size* for the categorical size system of the European Avalanche Warning Service. The analysis consists of two sample t-tests for the means of the three quantities. Table 3 contains the statistics and it is followed by the t-test results which were all calculated for separate variances of the groups.

Table 3: Data for calculation of two sample t-tests for differences in the means

Variable	No. avalanches	Mean	Std. dev.	Data set
$u_m(m/s)$	59	27	13	Canadian
$u_m(m/s)$	30	42	14	European-Japan
$\alpha(^o)$	59	34	4.3	Canadian
$\alpha(^o)$	29	28	3.6	European-Japan

size (1-5)	42	2.5	0.63	Canadian
size (1-5)	26	3.2	1.01	European-Japan

The t-test results showed statistically different means for the three variables. On average, the Canadian data had smaller u_m (p < 0.0005), larger α angles (p < 0.0005) and smaller *size* (p = 0.003). For the categorical *size* variable, we also included non-parametric the Mann-Whitney U test which gave $p = 0.001$.The medians for *size* were Canada (2) and European – Japan (3).The results suggest a consistency that the smaller Canadian avalanches have slower speeds and end up on steeper terrain, for the position of the tip of the debris, similar to the description of the α angle for runout suggested by Lied and Bakkehøi (1980) as explained in the Appendix. We feel the inclusion of smaller avalanches from Canada is important even though the speed data accuracy is not as good as for the larger avalanches from Europe-Japan. In consulting applications, small avalanches are important, particularly in Canada, since large avalanche paths are often avoided for placement of infrastructure, facilities and runout zone defenses. The smaller values of u_m for Canada are expected not just because of the *size* differences but also we believe the use of single values instead of a profile of values may provide underestimates of u_m in some cases.

Analysis of t-tests for terrain scales showed that the means of S_0 were not significantly different (p = 0.53): 1670 m (N =59) and 1580 (N=30) but the mean of H_0 was significantly higher (p < 0.005) for the Canadian data : 980 m (N=59) compared to the Europe – Japan data : 710 m (N=30).

8. Summary and conclusions

The approach here consists of empirical probability analysis of an extensive data set of maximum frontal speeds of flowing avalanches from 36 avalanche paths. Avalanche dynamics modelling presents huge challenges from a rational scientific perspective. The challenges include: unknown basal boundary conditions, unverified entrainment/deposition modelling, possible unknown effects of passive pressure and three dimensional terrain features. It is not possible to verify the parameters in avalanche dynamics models from field measurements alone and verified physical models for the parameters do not exist. Furthermore, it is not possible to calibrate a dynamics model without speed data (McClung and Schaerer, 1983). The empirical approach here may be relied on to place a constraint on modern complex avalanche dynamics models based on data and scaling for $S_o; H_0$ in regard to the design or maximum avalanche.

The scatter plots (Figs. 2,5,7,8) all show wide variations particularly in the middle portions where most data were taken. Some of this must be due to uncertainty in the data collection methods. However, some of it must be due to variability in avalanche motion which can include effects such as condition of the running surface, variations in mass including entrainment/deposition, water content/ temperature/ granulation effects (e.g. McClung and Schaerer, 2006: Steinkogler et al., 2015) and three dimensional terrain effects on dynamics including path confinement. It was not possible to include these effects explicitly in this paper. However, the asymptotic, empirical probabilistic approach here as in Section 3 (e.g. Fig. 2) may provide a scaled speed limit which includes some of these effects.

Modern consulting applications are often risk-based which imply probability concepts. The method used here introduces probability considerations into estimates of maximum speed scaled with path length scales based on runout. The design avalanche is often considered as that with highest speed or highest destructive effects and furthest runout. The analysis here contributes to definition of the design avalanche by providing maximum speed for a given stop position on an avalanche path.

The results based on α angle show, with significant speed data, that runout increases (α decreases) as maximum speed increases. However, the wide scatter (Figure 5) illustrates the complexity involved in avalanche dynamics. An α angle near 30^o may be achieved for maximum speeds from about 10 – 60 m/s. By definition, the α angle contains no length scale (only a ratio of length scales) which is a disadvantage and limits its predictive capability.

Correlation of α with S_0 and H_0 showed highly significant negative correlation with S_0 but insignificant correlation with H_0. Such might be expected since avalanche dynamics involves non-conservative path dependent (S_0) resistive forces. The variable H_0 is related to potential energy expenditure but avalanche motion does not consist simply of exchange of potential energy for kinetic energy. The 500 extreme avalanche runouts collected by McClung and Mears (1991) showed runout distances of more than 1000 m over ground with slope angles less than 10^o. For an average slope angle in the runout zone of 5^o with 1000 m horizontal reach beyond, the fall height in the runout zone would add 87 m to that from the 10^o point whereas addition to the path length would be 1000 m. Estimates of total path length traversed (S_0) would be a more accurate representation of energy loss than H_0. However, given the basic data sets presented here, we feel either S_0 or H_0 are avalanche path variables useful for simple speed scaling given the rough measure of runout that the α angle consists of. Our data, as well as the terrain information collected by McClung and Mears (1991), suggest that path geometry has a major effect on dynamics and runout.

Introduction of $size$ in terms of final deposit volume showed u_m increasing (Fig. 7) with $size$ but, again with wide scatter. For data rich $size\,3$, u_m varied from $11 - 56\ m/s$. For $size\,3$, large variations with α gave values from $24^o - 38^o$ (Figure 8).

The conventional approach to avalanche dynamics consists of solving for the speed all along the incline from start to final stop position. Whether one chooses α (Lied and Bakkehøi, 1980) as a measure of runout or S_0, the data and empirical analysis presented in this paper suggest highly significant challenges for the conventional approach in combination with field experimental and observational results. The latter reveal the importance of three dimensional effects, entrainment/deposition, ploughing at the front, character of the sliding surface, internal wave features and complicated flow regimes for dry avalanches (Schaerer and Salway, 1980; Gauer et al., 2008; Köhler et al., 2016), passive pressure and others. Verification is an essential scientific component of any model proposed.

Acknowledgements

The research of DMM was funded by the University of British Columbia. P.A. Schaerer contributed the Canadian speed data measured at Rogers Pass, British Columbia. The research of PG was financially supported by the Norwegian Ministry of Oil and Energy through project grant “R&D Snow avalanches 2017-2019” to NGI administered by the Norwegian Water Resources and Energy Directorate (NVE).

References

Bakkehøi, S, Domaas, U, Lied, K (1983) Calculation of snow avalanche runout distance, Ann, Glaciol. 4: 24 – 29.

Barbolini, M, Issler, D (2006) Avalanche test sites and research equipment in Europe: an updated overview. Final Report Deliverable D8. SATSIE Avalanche Studies and Model Validation in Europe.

Gauer, P, Issler, D, Lied, K, Kristensen,K, Sandersen, F (2008) On snow avalanche flow regimes: inferences from observations and measurements, International Snow Science Workshop, Whistler, B.C. Canada, Sept. 21 -27, 2008: 717 – 723.

Gauer, P (2013) Comparison of avalanche front velocity measurements: supplementary energy considerations, Cold Regions Sci. and Tech. 96: 17-22.

Gauer, P (2014) Comparison of avalanche front velocity measurements and implications for avalanche models, Cold Regions Sci. and Tech. 97: 132-150.

Gubler, H, Hiller, M, Klausegger, G, Suter, U (1986) Messungen an Fliesslawinen, Mittel. des Eidg. Inst. für Schnee und Lawinenforschung, 41 (August, 1986): 71 pp.

Harnett, DL (1975) Introduction to statistical methods, 2nd Ed., Addison-Wesley Publ. Co., Reading, MA, USA, 549 pp. + appendices.

Heim, A (1932) Bergsturz und Menschenleben, Geologishe Nachlese 30, Naturforschenden Gesellschaft, Zürich,77.

Köhler,A., McElwaine, JN, Sovilla, B, Ash, M, Brennen, P (2016) The dynamics of surges in the 3 February 2015 avalanches in Vallée de la Sionne, J. Geophys. Res. Earth Surf., 121, 2192 – 2210, doi:10.1002/2016JF0003887.

Körner, HJ (1980) Modelle zur Berechnung der Bergsturz- und Lawinenbewegnung. Interpraevent 1980 Band 2:15 -55.

Kotlyakov, VM, Rzhevskiy, BN, Samoylov, VA (1977) The dynamics of avalanching in the Khibins, J. Glaciol. 19(81) : 431 – 439.

Lied, K, Bakkehøi, S (1980) Empirical calculations of snow-avalanche run-out distance based on topographic parameters, J. Glaciol. 26 (94): 165 – 167.

McClung, DM (1990) A model for scaling avalanche speeds, J. Glaciol. 36 (123): 188-198.

McClung, DM, Mears, AI (1991) Extreme value prediction of snow avalanche runout, Cold Regions Sci. and Tech. 19: 163-175.

McClung, DM (2013) Effects of triggering mechanism on snow avalanche slope angles and slab depths from field data, Nat. Hazards 69:1721 – 1731, doi: 10.1007/s11069-013-0771-2.

McClung, DM , Schaerer, PA (1983) Determination of avalanche dynamics friction coefficients from measured speeds, Ann. Glaciol. 4**:** 170 – 173.

McClung, D, Schaerer, P (2006) The avalanche handbook, 3rd edn. The Mountaineers, Seattle, WA, 342 pp.

Schaerer, PA (1975) Friction coefficients and speed of flowing avalanches, Snow mechanics : Proceedings of the Grindelwald Symposium April, 1974, IAHS-AISH Publ. 114: 425 – 432.

Schaerer, PA, Salway, AA (1980) Seismic and impact-pressure monitoring of flowing avalanches, J. Glaciol. 26(94): 179 – 187.

Scheidegger, AE (1973) On the prediction of the reach and velocity of catastrophic landslides, Rock Mechanics 5 : 231-236.

Schleiss, V.G. (1989) Rogers Pass snow avalanche atlas, Glacier National Park, B.C. Canada, Environment Canada, Canadian Parks Service, Revelstoke, B.C. 313 pp.

Sovilla, B, Burlando, P, Bartelt, P (2006) Field experiments and numerical modelling of mass entrainment in snow avalanches, J. Geophys. Res. 111 (F3): doi: 10.1029/2005JF000391, F03007.

Steinkogler, W, Gaume, J, Löwe, H, Sovilla, B, Lehning, M (2015) Granulation of snow: from tumbler experiments to discrete element simulations, J. Geophys. Res. Earth Surf., 120,1107 – 1126, doi: 10.1002/2014JF003294.

UNESCO (1981) Avalanche Atlas, Internat. Comm. on Snow and Ice, IAHS Press, Wallingford, Oxfordshire, UK.

Vogel, RW, McMartin, DE (1991) Probability plot, goodness-of-fit and skewness estimates for the Pearson type 3 distribution, Water Res. Research 27: 3149 – 3158.

Appendix: Interpretation of α angles

The α angle was introduced as a simple measure of runout by Heim (1932) and Scheidegger (1975) and Körner (1980) for landslides, rock avalanches and flowing avalanches. The latter 2 authors connected it to centre-of-mass avalanche dynamics models. Lied and Bakkehøi (1980) introduced the α angle as an index for empirical runout. They defined it as sighting from the distal end or tip of the avalanche runout position to the top position of the start zone. For empirical runout, they defined it for maximum runout position for return periods on the order of about 100 years where normally return period means average time between events reaching or exceeding a given location. In this paper, the same definition used by Lied and Bakkehøi (1980) is used. However, the α angles reported here are determined from the distal (downslope end) of the individual avalanche deposits not maximum runout positions for the paths

If an avalanche path profile is defined by a curve $y = f(x)$ with y as the ordinate and x as the abscissa then the α angle is defined simply by the slope along the path averaged in the x direction:

$$\tan\alpha = \frac{1}{X_0}\int_0^X \frac{dy}{dx}dx = \frac{1}{X_0}\int_{H_0}^0 dy = \frac{H_0}{X_0} \qquad \text{(A1)}$$

where the beginning and end (x,y) coordinate pairs are : $(0, H_0)$ and $(X_0, 0)$ with H_0 as total vertical drop and X_0 as total horizontal reach and $dy = -|dy|$. Clearly the α angle is devoid of scale as its definition involves a ratio of length scales.

The interpretation of the α angle envisioned by Lied and Bakkehøi (1980) is that lower α angles imply longer runout for a path in the sense that the avalanches reach further into the valley where lower slope angles are generally found. Lied and Bakkehøi (1980) found good fits to their path profiles using a parabola: $y = ax^2$. Bakkehøi, Domaas and Lied (1983) used an improved model: $y = ax^2 + bx + c$ to fit 206 avalanche path profiles from western Norway. Use of the latter profile in equation (A1) with : $(dy/dx)_{x=0} = -\tan\psi_i; (dy/dx)_{x=X_0} = -\tan\psi_f$ gives:

$$\tan\alpha = \frac{1}{2}\left(\tan\psi_i + \tan\psi_f\right) \qquad \text{(A2)}$$

where ψ_i is the initial start zone angle and ψ_f is the final stop angle.

Equation (A2) is not a model. It is only a means of illustrating the meaning of the α angle in a rough sense. However, it shows simply for paths with monotonically decreasing slope angle from the start that increasing stop angle ψ_f implies higher α angle. McClung and Schaerer (1983) listed ψ_f in the range $0^o - 34^o$ for 38 avalanches at Rogers Pass, B.C. The most probable value of $\psi_i = 38^o$ for hundreds avalanches from fracture line profiles was reported by McClung (2013). Use of $\psi_i = 38^o$ with the range of stop angles above gave: $22^0 < \alpha < 36^0$. Except for 2 avalanches with $\alpha = 45^0$, the range of α angles for the Rogers Pass data here (57 values) is: $24^0 - 40^0$ and 97% of the full data set (Fig. 3) are in the same range so the simple explanation (A2) is in rough agreement. The analysis in (A2) will not apply to some paths at Rogers Pass, since some profiles show steeper sections below the start area than in the start area (Schleiss, 1989) whereas the illustrative 2nd degree parabola implies gradually decreasing steepness all along the path.